

# A torsion balance as a weak-force testbed for novel optical inertial sensors

Gerald Bergmann<sup>1,2,3</sup> , Carolin Cordes<sup>1,2</sup> ,  
Christoph Gentemann<sup>1,2</sup> , Vitus Händchen<sup>1,2,4</sup>,  
Wang Qinglan<sup>1,2,5</sup> , Hao Yan<sup>1,2,6</sup>, Karsten Danzmann<sup>1,2</sup>,  
Gerhard Heinzel<sup>1,2</sup>  and Moritz Mehmet<sup>1,2,7,\*</sup> 

<sup>1</sup> Max Planck Institute for Gravitational Physics (Albert Einstein Institute),  
D-30167 Hannover, Germany

<sup>2</sup> Leibniz Universität Hannover, D-30167 Hannover, Germany

E-mail: [moritz.mehmet@aei.mpg.de](mailto:moritz.mehmet@aei.mpg.de)

Received 11 September 2023; revised 21 January 2024

Accepted for publication 15 February 2024

Published 5 March 2024



CrossMark

## Abstract

Torsion balances (TBs) are versatile instruments known for their ability to measure tiny forces and accelerations with high precision. We are currently commissioning a new TB facility to support the development and testing of novel optical inertial sensor units for future gravity-related space missions. Here, we report on the status of our apparatus and present first sensitivity curves that demonstrate acceleration and torque sensitivities of  $5 \cdot 10^{-11} \text{ ms}^{-2}$  and  $1 \cdot 10^{-12} \text{ Nm} \sqrt{\text{Hz}}^{-1}$  at frequencies around 4 mHz, respectively. Capacitive sensors and optical levers measure the dynamics of the system with a displacement sensitivity of down to  $9 \cdot 10^{-10} \text{ m} \sqrt{\text{Hz}}^{-1}$  for the former and  $2 \cdot 10^{-11} \text{ m} \sqrt{\text{Hz}}^{-1}$  for the latter. Combining the readout of the suspended

<sup>3</sup> Current address: Deutsches Zentrum für Luft- und Raumfahrt (DLR) Institut für Satellitengeodäsie und Inertialsensorik, D-30167 Hannover, Germany.

<sup>4</sup> Current address: Lugensa GmbH, D-22087 Hamburg, Germany.

<sup>5</sup> Current address: School of Mathematics, Physics and Optoelectronic Engineering, Hubei University of Automotive Technology, Shiyan 442002, People's Republic of China.

<sup>6</sup> Current address: MOE Key Laboratory of Fundamental Physical Quantities Measurement and Hubei Key Laboratory of Gravitation and Quantities Physics, PGMF and School of Physics, Huazhong University of Science and Technology, Wuhan 430074, People's Republic of China.

<sup>7</sup> Current address: Texas A&M University, Department of Physics & Astronomy, College Station, TX 77843, United States of America.

\* Author to whom any correspondence should be addressed.



Original Content from this work may be used under the terms of the [Creative Commons Attribution 4.0 licence](https://creativecommons.org/licenses/by/4.0/). Any further distribution of this work must maintain attribution to the author(s) and the title of the work, journal citation and DOI.

inertial member (IM) with environmental sensor signals, the system is characterized, and limiting noise sources are identified. We find that, in particular, the coupling of ambient seismic motion is limiting over a broad frequency range and show that due to its high susceptibility to ground motion, our TB is also a promising platform for exploring ground motion sensing in multiple degrees of freedom. Future upgrades will focus on mitigating seismic noise by controlling the torsion fiber suspension point using piezoelectric actuators and the integration of precision interferometric readout of the IM. These improvements will further increase the sensitivity towards the thermal noise limit which constrains the performance to  $1 \cdot 10^{-13} \text{ ms}^{-2} \sqrt{\text{Hz}}^{-1}$  at 4 mHz.

Keywords: torsion balance, inertial sensing, capacitive readout, optical lever, seismic sensing

## 1. Introduction

The underlying principle of gravity-related satellite missions, such as GRACE-FO [1, 2], MICROSCOPE [3], LISA-Pathfinder (LPF) [4, 5], and LISA [6], is sensing the purely gravity-driven motion of freely floating test masses (TMs). To control the spacecraft and to distinguish locally induced noise from the science signal, the position and orientation of the satellite with respect to the TM need to be measured. Typically, this readout is done electrostatically via a set of electrodes surrounding the TM, as realized, for example, in the accelerometers for the GRACE-FO and MICROSCOPE satellites [7, 8] or the LPF gravitational reference sensor (GRS) [9].

The LPF mission has demonstrated that laser interferometric readout offers the opportunity to enhance the sensitivity of detecting freely floating TMs in space [10, 11]. However, due to its relatively large interferometric setup the LPF readout scheme would not be suitable for a GRS-type inertial sensor requiring the readout of additional degrees-of-freedom (DoF). However, novel optical readout techniques have a high potential to improve the sensitivity of inertial sensors while requiring relatively little space. Experiments have shown that, for instance, deep frequency modulation (DFM) interferometry [12, 13] could be a suitable candidate for TM readout [14, 15]. This technique combines the high sensitivity of interferometric displacement sensing with a large dynamic range. Furthermore, the optical topology can be kept extremely compact, which would allow for incorporating multiple optical sensors in a relatively small accelerometer unit.

The main challenge in developing and improving high-precision sensor systems for gravitational space projects on ground is the presence of much larger forces compared to the conditions in orbit. Factors such as the presence of 1 g gravity and seismic motion in the laboratory necessitate a suitable experimental setup for simulating, to some extent, the weak force environment experienced inside a satellite. This can be accomplished through the use of a torsion balance (TB). For several decades, TBs have been developed to a very high degree of sophistication for experiments that require the absence of large disturbances in order to enable the measurement of tiny forces and accelerations. Such experiments include, for example, tests of the equivalence principle [16], measurements of the gravitational constant  $G$  [17–19], testing the inverse square law [20, 21], probing the gravitational coupling between miniature masses [22] and the observation of noise created by fluctuating electrostatic charges on dielec-

tric surfaces [23]. TBs have also proven crucial during the development and verification of the GRS for the LPF mission [24–26] and have been employed to design simplified versions of this device [27–29].

Here, we introduce a new TB which is currently being commissioned at Leibniz Universität Hannover and the Max-Planck Institute for Gravitational Physics (Albert Einstein Institute). This facility will serve as a low-noise test platform for evaluating and improving the performance of novel high-precision sensing and control units for TM read out. To advance existing techniques such as DFM interferometry into integrated inertial sensor units, the proximity of a suitable test bed is essential. Our system offers ample space for the integration of GRS-type inertial sensors based on multichannel interferometric readout. In this article we provide a general overview of the current status of our device and present the first sensitivity curves. As anticipated, the science signal is dominated by seismic noise over a wide frequency range. In the future, we will mitigate this limitation, but for now we make use of it to investigate the potential of realizing a multi-DoF ground motion sensor.

## 2. The Hannover TB (HTB)

In principle, the TB is simply an inertial member (IM) suspended from a wire. The rotational stiffness about the vertical axis of such a system is, in first order, independent of gravity, and thus can be tuned to a fairly low resonance frequency  $f_0$  by altering the system geometry. At frequencies well above  $f_0$ , the torsional motion of the IM is strongly decoupled from the environmental motion. In the absence of other external forces, the IM follows the suspension point motion in the frequency band below the resonance frequency. Figure 1 depicts the conceptual design of the apparatus. When designed in a way that the TMs are far away from the rotational axis, for instance in a cross configuration as shown in figure 1(b), the torsional motion of the IM translates in first order to translational motion of the TMs. The extremely low restoring torque of this mechanical harmonic oscillator makes the TMs highly susceptible to external low-frequency forces. These properties allow for simulating the behavior of a free-falling TM down to the mHz regime in one translational degree of freedom. Consequently, the influence of low force noise sources on the TM and the operation of inertial sensor units in such an environment can be tested.

As shown in figure 1(a), the IM is suspended from a  $50\ \mu\text{m}$  thick, 1.2 m long tungsten fiber inside a 600 liter vacuum envelope. On the top, the torsion fiber is connected to an eddy current damper to weaken non-torsional modes. The eddy current damper in turn is suspended from a 0.2 m long pre-hanging fiber with a diameter of  $150\ \mu\text{m}$  which is connected at its upper end to a mechanical vacuum feed-through (not shown) that enables us to adjust the angular position and height. A pressure of about  $5 \cdot 10^{-8}$  mbar is reached in a time span of about two days using a turbo-pump. To create a low-vibration environment, this pump is switched off during high-precision measurements and low pressure is maintained by an ion getter pump. The necessary scroll pump for generating pre-vacuum is situated in an adjacent room whose foundation is separated from the laboratory to reduce acoustic and vibration coupling. The entire chamber is supported by three feet with heavy-duty piezo actuators (PZTs) which are mounted on a rigid steel construction. As shown in detail in figure 1(b), the baseline design of the IM is a cross-bar with cubes attached to the ends of four arms that mimic the free-floating inertial sensor TMs which are to be decoupled from the lab environment as good as possible. Each of the cubic TMs has a side length of 3 cm and a mass of approximately 73 g. Aluminium rods with balancing

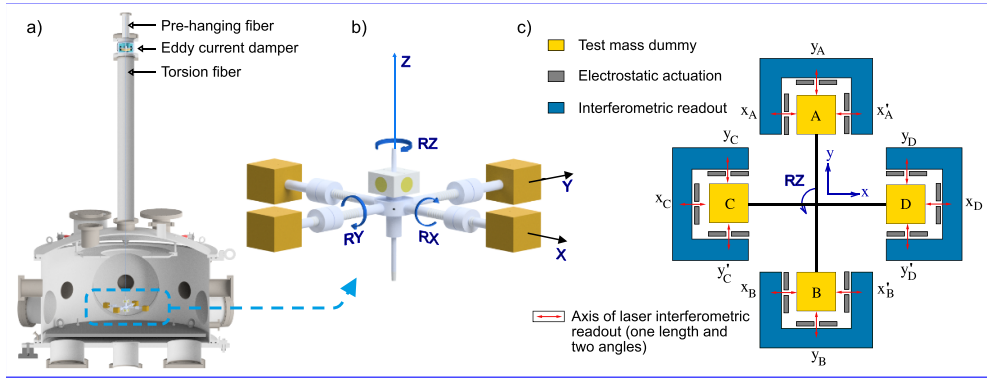


**Figure 1.** (a) Cross-section of the baseline design of the HTB vacuum chamber. The pre-hanging fiber and the eddy current damper are located in the tube that makes up the top of the chamber. The lower part of the chamber contains the suspended inertial member as well as all the flanges, viewports and the base plate for the optical equipment. (b) CAD drawing of the 4-arm inertial member and definition of the coordinate system. The inertial member is suspended from the fiber and consists of a block with mirrors for the optical levers in the middle and four arms with the TMs at the end. (c) Preliminary sketch of a GRS-type readout system including interferometric sensors, which could be added from multiple sides, for example, through holes in the capacitor plates.

nuts connect the TMs to the center-piece of the IM. The armlength, i.e. the distance from the torsion fiber to the center of a TM is 13 cm. Figure 1(c) depicts a possible implementation of multi-channel interferometric readout integrated with electrostatic actuation to realize a GRS-type inertial sensor enclosing the freely floating TMs. Each interferometric readout axis would provide access to one length and two angles, i.e. the TM displacement along that axis (via the interferometric phase) and the corresponding pitch and yaw (via differential wavefront sensing), respectively.

Since seismic motion can be a limiting noise source in TB measurements over a wide frequency band, three seismometers [30] (not shown in figure 1) are installed on top of the vacuum chamber lid that continuously record seismic noise in our setup. Temperature variations, as well as fluctuations of the magnetic field, are expected to influence the motion of the TMs with respect to the sensors. A set of temperature sensors, located both inside the vacuum enclosure and outside and a magnetometer [31] are located close to the pendulum to verify the coupling of these environmental noise sources. The data of all sensors is continuously recorded and perpetually stored by a LIGO-like control and data acquisition system (CDS) [32]. This enables a quick and easy analysis of the coupling and the realization of control loops.

### 2.1. Sensors and actuators

It is essential to measure the TM dynamics using methods other than the inertial sensors to be tested for several reasons: for the characterization of the mechanical behavior of the system during the commissioning phase, for the control of the IM's motion, and for the use as witness sensors for the verification of measurements during the testing of novel sensors.

For simplicity, the first version of our IM was chosen to be a dumbbell with two TMs only, as shown in figure 2.

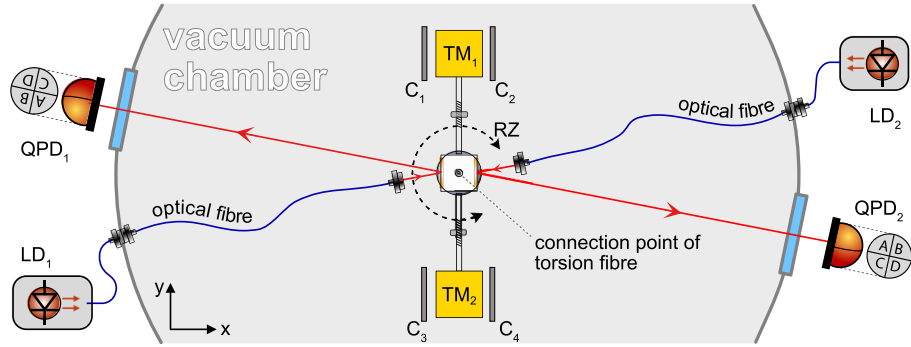


**Figure 2.** Schematic of the setup. Inside the vacuum chamber, two TMs ( $TM_1$  and  $TM_2$ ) are rigidly connected to a center-piece with aluminum rods. This dumbbell is suspended from the torsion fiber which connects to the top of the centerpiece. Balancing nuts on each rod are used for levelling the vertical position. Electrode plates are used to sense the position of the TMs via a change of capacitances  $C_1$  to  $C_4$ . Two optical levers are created by reflecting the beams of two laser diodes ( $LD_1$  and  $LD_2$ ) off gold mirrors attached to opposing sides of an aluminum cube that is mounted on top of the centerpiece. The position change of the two laser beams is monitored with quadrant photo detectors ( $QPD_1$  and  $QPD_2$ ) in transmission of optical windows.

The HTB's first optical sensor comprises a pair of optical levers (OLs). Two laser beams are fiber-coupled into the vacuum chamber and reflected off opposing mirrors positioned approximately 3 cm above the center of mass of the structure. The reflected light passes through viewports and is detected by segmented quadrant photodetectors (QPDs) rigidly mounted outside the vacuum chamber. The motion of the light spots on the QPDs is dominated by the angular and translational differential motion between the IM and the vacuum chamber. By properly combining the QPD signals of the two OLs, the sensor can distinguish the signal due to horizontal displacement ( $X$ ) from the contribution of torsional ( $RZ$ ) and roll ( $RY$ ) motion, respectively (see figure 1(b)). Despite its simplicity, this motion sensor is highly sensitive, reaching a sensitivity of  $1.5 \cdot 10^{-10} \text{ rad } \sqrt{\text{Hz}}^{-1}$  and a dynamic range of approximately 1 mrad.

In addition to the OLs the HTB is equipped with a set of capacitive (CAP) sensing and actuation units realized by aluminium plates (P1 to P4) with a side length of about 3.5 cm placed at a distance of 5 mm in horizontal ( $X$ ) direction next to the two TMs. With a 10 V AC voltage at 6 kHz applied to the TM, each of the two faces of one TM in this DoF and one of the aluminium plates then behave as an effective plate capacitor. For a small change  $\Delta x$  of the distance between one plate and the TM, the distance of the TM to the second plate changes by  $-\Delta x$ . The setup can be considered as two plate capacitors with capacitances of  $C_{\pm}(\Delta x) = \epsilon_0 \epsilon_r \cdot \frac{A}{d_0 \mp \Delta x}$ . To first order, this leads to a change  $C_{\pm} = C_0(1 \pm \frac{\Delta x}{d_0})$  in capacitance on either side of the test mass and a change in the capacitance difference  $\Delta C = C_+ - C_- = C_0 \frac{2\Delta x}{d_0}$ , accordingly again to first order, which makes it possible to measure small changes  $\Delta x$  electrostatically in a linear regime. From the capacitor distance and TM size, a value of 1.6 pF is expected for  $C_0$ . The two capacitor plate pairs can be used to distinguish between horizontal and torsional motion. To this end, the respective signals from each pair of capacitors are subtracted with a commercial differential amplifier and band-pass filter (Stanford Research Systems SR560),

digitized and demodulated with the 6 kHz signal. Since the two TMs are moving in the same direction relative to the capacitor plates for the X motion and in opposing directions for the RZ motion, one can add or subtract the CAP sensing signal of TM<sub>1</sub> and TM<sub>2</sub> and divide them by two to separate the signals for translation in X (CAP<sub>X</sub>) and rotation around the vertical axis (CAP<sub>RZ</sub>), respectively. All payload sensors (OL and CAP) were calibrated to the seismometer signal. This calibration was verified by the OL beam displacement on the QPDs. The deployed sensors naturally measure the IM motion with respect to the chamber motion. Regarding the TB as an ideal multidimensional mechanical harmonic oscillator, the sensor signals in the individual DoFs are dominated by chamber motion above the corresponding resonance frequency. In the frequency range far below this frequency, the payload follows the motion of the chamber so that the sensor signal asymptotically approaches zero.

The capacitor units are also used to actively control the TM position in one DoF by applying a low-frequency voltage ( $\ll 6$  kHz) to the non-segmented aluminium plates. The frequency splitting between the sensing and actuation signal is realized by analog electronics in front of the differential amplifier that enables us to connect the plates to an analog output of the CDS with only minimal degradation of the sensing signal. A feedback signal is generated with the CDS by implementing a digital control loop with unity gain frequency of approximately 100 mHz. This control loop is used to damp the free motion of the pendulum until the equilibrium position is reached. It is switched off during the measurements presented below.

### 3. Current status, results and limitations

As mentioned above, only two of the four TMs are currently installed on the HTB's IM. This has allowed for easier development and testing of the system without greatly affecting its basic behavior. With the aid of the above-described sensors, the mechanical properties and the coupling of noise sources have been investigated. The results are discussed in this section.

Figure 3 shows the amplitude spectral density of the data measured with the two OLs and the two CAP units.

The data of each sensor type are combined to obtain the differential tank-to-TM motion in the torsional direction. Both, the angular motion and the corresponding TM motion are shown in the plot (conversion factor:  $l = 13$  cm). With the help of an analytical and a finite element model of the system, the individual resonance peaks were identified: the torsional mode at 0.5 mHz, the two swing modes at 380 mHz, the pitch mode at 1.1 Hz, the bounce mode at 7.9 Hz and the roll mode at 9.1 Hz. Also, motion induced by bounce and tilt modes of the entire vacuum chamber sitting on PZT feet and the supporting structure was identified around 10 Hz. The violin modes of the torsion fiber are estimated to be at frequencies higher than 120 Hz. At high frequencies, the OL is limited at  $2 \cdot 10^{-11} \text{ m} \sqrt{\text{Hz}}^{-1}$  by sensor noise. At 100 mHz rotational motion of the chamber is suspected to limit the measurement to  $9 \cdot 10^{-10} \text{ m} \sqrt{\text{Hz}}^{-1}$ . Below 10 mHz, the CAP and OL measurements agree well. The discrepancy in mode content and amplitude of the two signals between 10 mHz and 10 Hz is caused by the different degree of cross coupling from the non-torsional DoFs to the sensors. While the OL is primarily a sensor for angular motion, the two sets of capacitors sense the horizontal displacement of the TMs. Imperfection and structural differences between the two CAP units cause coupling of the horizontal swing motion to the capacitance. Between 100 mHz and 10 Hz the CAP signal shows significant coherence to horizontal chamber motion measured with the seismometers, as verified by a signal analysis in the CDS. In comparison, the horizontal ground motion coupling to the OL signal is low, which is described in more detail in section 3.1. The pitch mode motion of the payload at 1.1 Hz couples relatively strongly to the OL measurement, probably due to

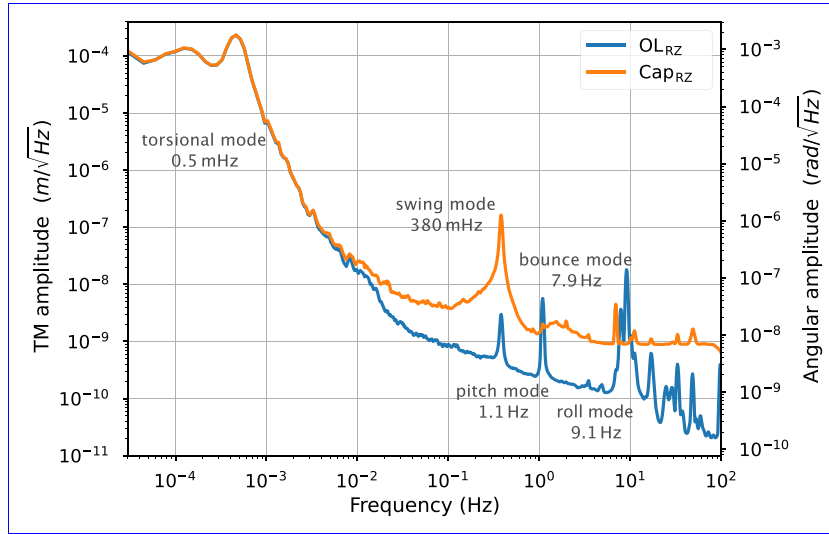


**Figure 3.** HTB performance: the differential motion between the test mass and the vacuum chamber (i. e. ground) is read out with two sets of sensors: the optical levers (OL) and the capacitive sensors (CAP). The OL reaches a sensitivity of  $1.5 \cdot 10^{-10} \text{ rad} \sqrt{\text{Hz}}^{-1}$ , however, its dynamic range is limited. The high dynamic range CAP senses the differential motion between ground and TM down to  $7 \cdot 10^{-9} \text{ rad} \sqrt{\text{Hz}}^{-1}$ .

geometrically imperfect alignment. Above 40 Hz the CAP measurement is limited by sensor noise.

The displayed measurements were deliberately recorded at a moderate gas pressure of  $10^{-2}$  mbar at which the pendulum damping is dominated by viscous rest gas damping. The resulting torsional quality factor of  $Q_v = 8$  simplifies the ongoing construction and commissioning of the HTB. In a  $5 \cdot 10^{-8}$  mbar gas pressure environment, a quality factor of  $Q_s = 2500$  was achieved. Figure 4 depicts the current limit for the measurement of external acceleration and torque acting on the TMs. The sensitivity of the CAP (orange) and OL (blue) sensing scheme are derived from the torsional measurements (data shown in figure 3) as  $\text{Acc}_{\text{RZ}} = X_{\text{RZ}} \omega^2 / (1 - H_{\text{RZ}})$ , where  $X_{\text{RZ}}$  is the displacement measurement,  $\omega$  is the angular frequency, and  $H_{\text{RZ}}$  is the transmissibility function of a simple, in this low Q case viscously damped, harmonic oscillator with the torsional resonance frequency of the HTB and the corresponding Q-factor  $Q_v = 8$ . To convert acceleration into torque, we multiply by the ratio of the IM's moment of inertia and armlength ( $I_z/l$ ). Both the OL and the CAP measure acceleration down to  $5 \cdot 10^{-11} \text{ m s}^{-2} \sqrt{\text{Hz}}^{-1}$  at 4 mHz, which corresponds to a torque of  $10^{-12} \text{ Nm} \sqrt{\text{Hz}}^{-1}$ . In this frequency band, the sensors' signals are highly coherent and therefore likely to be dominated by differential rotation between IM and chamber.

A typical low frequency noise source is temperature fluctuations. The influence of temperature fluctuations on the IM sensor signals is tested with a set of temperature sensors. Figure 5 shows typical temperature measurements inside and outside the vacuum chamber during the week and on a weekend. Inside the vacuum chamber, a temperature stability of about  $11 \text{ mK} \sqrt{\text{Hz}}^{-1}$  at  $50 \mu\text{Hz}$  is achieved. The slightly higher temperature fluctuations of about  $49 \text{ mK} \sqrt{\text{Hz}}^{-1}$  at  $50 \mu\text{Hz}$  on weekdays are mainly caused by human activity in the vicinity of the experiment. The coherence between the temperature sensor signal inside the vacuum

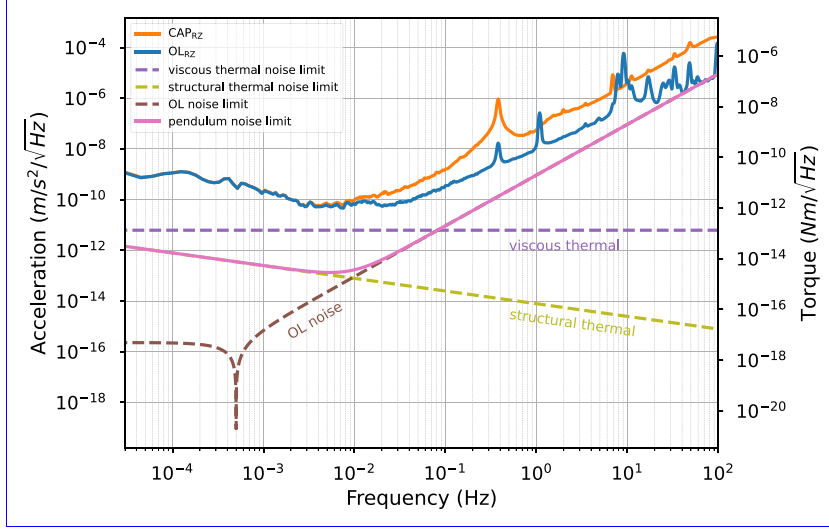


**Figure 4.** HTB thermal noise budget compared to measurements. Acceleration and torque noise spectral densities of the optical lever (blue) and capacitive (orange) sensing schemes were derived from the respective displacement data as shown in figure 3. The conversion factor between acceleration and torque is  $I_z/l$ . Both sensing schemes reach  $5 \cdot 10^{-11} \text{ ms}^{-2} \sqrt{\text{Hz}}^{-1} \cong 1 \cdot 10^{-12} \text{ Nm} \sqrt{\text{Hz}}^{-1}$  at frequencies around 4 mHz. Dashed curves show the estimated contributions of the optical lever (OL) and the thermal noise for viscous and structural damping, i.e. for the low and high Q regime, respectively. The sum of OL noise and thermal noise in case of structural damping yields the pendulum noise limit (magenta) for our current configuration, which reaches  $1 \cdot 10^{-13} \text{ ms}^{-2} \sqrt{\text{Hz}}^{-1} \cong 2 \cdot 10^{-15} \text{ Nm} \sqrt{\text{Hz}}^{-1}$  at 4 mHz.

chamber and the IM sensor signals increases at low frequencies (see figure 6). This indicates that temperature variations only significantly affect the measurement of IM dynamics below the HTB fundamental resonance frequency. On weekends, the influence of temperature variations is greatly reduced compared to weekdays.

The dashed curves in figure 4 show the estimated contributions of the optical lever and the thermal noise limited sensitivity for viscous and structural damping, i.e. for the low and high Q regime, respectively. To calculate the thermal noise contribution we used the formula for displacement thermal noise due to damping as given in [33]. Adapting this for angular displacement yields

$$\tilde{\theta}_{\text{therm}}^2(f) = \frac{4k_B T \varphi(f)}{(2\pi f) (2\pi f_0)^2 I_z \left[ \left( 1 - \left( \frac{2\pi f}{2\pi f_0} \right)^2 \right)^2 + \varphi(f)^2 \right]}, \quad (1)$$

where  $k_B$  is the Boltzmann constant,  $T$  is the temperature in Kelvin, and  $I_z$  is the IM's moment of inertia. The loss angle  $\varphi(f)$  differs for the two damping regimes:  $\varphi_v(f) = f/(f_0 \cdot Q_v)$  for viscous damping and depends on the measurement frequency  $f$  and resonance frequency  $f_0$ .

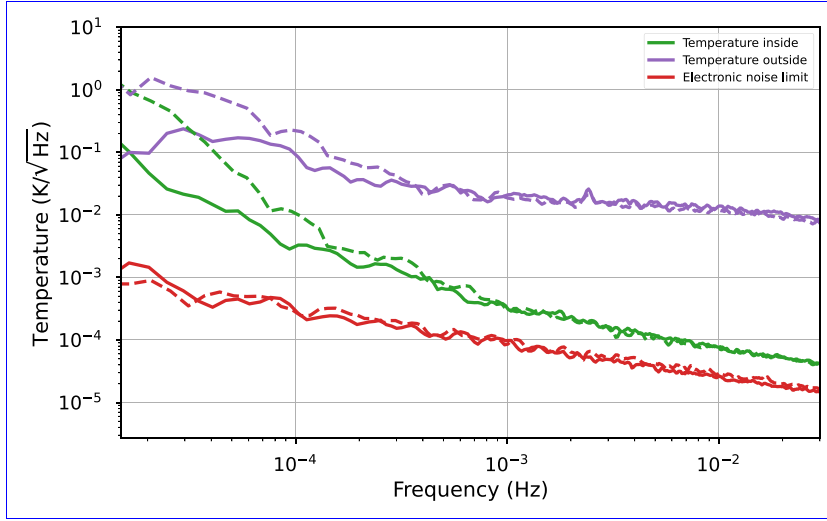


**Figure 5.** Typical temperature measurement inside (green) and outside (purple) the vacuum chamber compared to the temperature readout noise (red). The low frequency temperature fluctuations during the week (dashed lines) are significantly higher than during a weekend (solid lines).

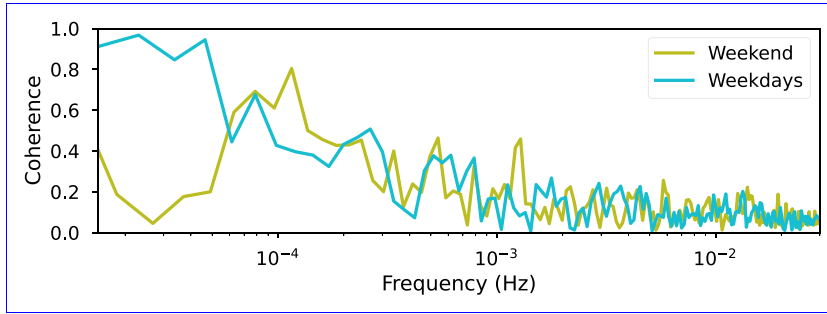


**Figure 6.** Coherence between the temperature sensor inside the vacuum chamber (see figure 5) and the CAP<sub>RZ</sub> signal. The measurements indicate that the motion induced by temperature variations dominates the HTB dynamics only at low frequencies. In the weekend measurement, the temperature influence is strongly reduced due to the higher temperature stability.

For structural damping the loss angle  $\varphi_s(f) = 1/Q_s$  is constant. This can be converted to an acceleration noise limit in the same way as the OL and CAP measurements were treated:

$$\tilde{a}_{\text{therm}}(f) = \sqrt{4k_B T \frac{(2\pi f_0)^2 l^2}{(2\pi f) I_z} \varphi(f)}, \quad (2)$$

where  $l$  is the armlength of the IM. To derive the pendulum noise limit (magenta curve in figure 4) we chose a torsional quality factor of  $Q_s = 2500$ , which was achieved at a vacuum pressure below  $10^{-7}$  mbar. At this low pressure, the oscillation loss is limited only by structural

**Table 1.** Important physical parameters of the torsion pendulum.

Mean laboratory temperature ( $T$ )	21 °C
Torsion fiber radius ( $r$ )	25 $\mu\text{m}$
Fiber length ( $L$ )	1.2 m
IM arm length ( $l$ )	13 cm
Moment of inertia ( $I_z$ )	$2.8 \cdot 10^{-3} \text{ kg m}^2$
Young's modulus of Tungsten ( $E$ )	400 GPa
Poission's ratio of Tungsten ( $\nu$ )	0.28
Shear modulus of Tungsten ( $G = \frac{E}{2(1+\nu)}$ )	156.25 GPa
Torsional stiffness ( $\kappa = \frac{GJ}{L} = \frac{G\pi r^4}{2L}$ )	$8 \cdot 10^{-8} \text{ N m}$
Torsional resonance frequency ( $f_0 = \frac{1}{2\pi} \sqrt{\frac{\kappa}{I_z}}$ ), calculated	$8 \cdot 10^{-1} \text{ mHz}$
Torsional resonance frequency, measured	$5 \cdot 10^{-1} \text{ mHz}$

damping. Assuming the system was limited solely by the corresponding thermal noise contribution and the OL-readout noise, our facility should enable the sensing of external accelerations down to  $1 \cdot 10^{-13} \text{ m s}^{-2} \sqrt{\text{Hz}}^{-1} \cong 2 \cdot 10^{-15} \text{ Nm} \sqrt{\text{Hz}}^{-1}$  at 4 mHz. The OL contribution was derived by the readout noise measured at 40 Hz. Table 1 summarizes the relevant physical quantities used to describe our apparatus.

Figure 4 also shows the thermal noise limit in the case of viscous damping, which is dominant at  $10^{-2}$  mbar, and is plotted for comparison. The amplitudes of the measured acceleration are well above these noise limits as external perturbations such as seismic, thermal deformation of the experimental setup, magnetic and electrostatic coupling and the cross-coupling from the non-torsional degrees of freedom, especially at the mechanical resonances, are likely dominating the signal.

When projecting the HTB noise to a heavier TM with the mass  $m_{\text{sm}}$  it scales with the mass ratio  $m_{\text{eff}}/m_{\text{sm}}$ , where  $m_{\text{eff}} = I_z/l^2 \approx 166 \text{ g}$  is the effective mass of the HTB. For comparability to other TB sensitivities, reported for example in [24, 25, 27, 34], the acceleration noise limit for a TM as planned for the LISA space mission with  $m_{\text{sm}} = 1.9 \text{ kg}$  would be  $1 \cdot 10^{-14} \text{ m s}^{-2} \sqrt{\text{Hz}}^{-1}$  at 4 mHz, accordingly.

### 3.1. The HTB as motion sensor

As mentioned above, one of the major noise sources coupling into the measurement is ground motion dominating the chamber motion. When regarding this detected motion not as noise but as signal, it transforms the HTB into a multi-degree of freedom seismometer with high sensitivity at low frequencies, in particular in the angular DoF around the vertical axis.

Among other applications, multi DoF low-frequency ground motion sensors are of high interest for ground-based gravitational wave detection and seismology. Current ground-based gravitational wave detectors are limited at low frequencies by seismic coupling to the suspended TMs [35]. Therefore, deploying motion sensors for active isolation is crucial, and the low-frequency performance of such devices will directly influence the measurement band of the gravitational wave detectors. Numerous novel motion sensors are the subject of investigation to enable the desired low-frequency performance of future ground-based gravitational wave detectors such as the Einstein telescope [36, 37].

In order to obtain the ground motion information from our measurements, the system's description is simplified as a multi-DoF structurally and viscously damped harmonic oscillator, and the ground motion coupling is computed accordingly. The ground motion induced IM

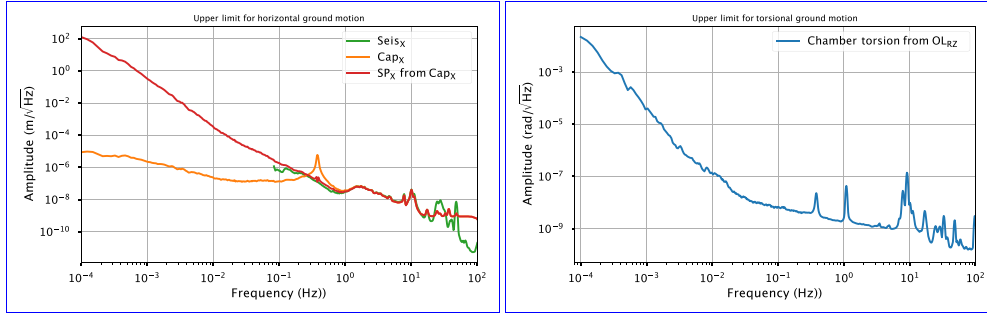


**Figure 7.** Upper limit for ground motion measured with the HTB. Left: differential horizontal motion between chamber and inertial member (orange) and the suspension point motion derived from it (red) compared to the chamber motion measured with the seismometers (green). The seismometer and the CAP data are coherent over a wide spectral range. Right: torsional ground motion upper limit derived from the OL measurement.

motion is simply  $\vec{x}_p = H^{TB} \vec{x}_g$ , where  $\vec{x}_p$  and  $\vec{x}_g$  are the 6 DoF IM and ground motion and  $H^{TB}$  is the transmissibility matrix from ground to IM motion. The diagonal elements of  $H^{TB}$  can be regarded as 6 DoF harmonic oscillator transmissibility functions with

$$H_{jj}^{TB} = \left( 1 - \frac{f^2}{f_{0j}^2} \frac{1}{1 + i(\varphi_{s_j}(f) + \varphi_{v_j}(f))} \right)^{-1}, \quad (3)$$

where  $f_{0j}$  are the resonance frequencies in the 6 DoF.  $\varphi_{s_j}$  and  $\varphi_{v_j}$  are the corresponding loss angles describing the structural and the viscous damping. This simplification does not regard the cross-coupling between the DoFs. Since the sensors are rigidly connected to the chamber and thereby measure the relative motion between the IM and the chamber, neglecting other limitations, the ground motion can be deduced as

$$\vec{x}_g = \frac{\vec{x}_s}{1 - H^{TB}}, \quad (4)$$

where  $\vec{x}_s$  are the sensor signals. For  $f > f_{0j}$ ,  $\vec{x}_s$  converges to  $\vec{x}_g$ . This enables high sensitivity ground motion sensing above the mechanical resonances.

Figure 7 shows an upper limit of the ground motion deduced from the CAP and the OL data in one horizontal DoF and in the torsional DoF. The orange curve in figure 7(left) represents the differential TM to ground motion in the X-direction measured with the CAP. By filtering this data based on a simple harmonic oscillator model, an upper limit for the horizontal ground motion can be deduced (red). Between 1 mHz and 20 Hz the two independent horizontal measurements of OL and CAP are coherent. This indicates that in this frequency band the two sensors are not noise limited, but measure real motion. Both sensor signals are furthermore highly coherent to the horizontal motion signal recorded by the seismometers between approximately 100 mHz and 20 Hz, which indicates with high confidence accurate horizontal ground motion sensing in this frequency band. Above 20 Hz sensor noise limits the measurement.

Below approximately 100 mHz all typical horizontal seismometers are dominated by a tilt ground motion coupling proportional to  $g/\omega^2$  [38]. This should be the case for the HTB as well. In principle, the tilt motion of the system should be detected by the vertical component of the

OL sensors. Due to technical difficulties, the sensitivity of this OL signal was not sufficient at the time of writing. Further commissioning of the sensor should allow for ground tilt sensing in the frequency band below approx. 100 mHz, where the horizontal HTB signals are expected to be dominated by ground tilt. This, in turn, would allow the measurement of tilt-free horizontal ground motion by subtracting the two signals.

Figure 7(right) shows the upper limit for torsional ground motion in our laboratory, measured by the OL. Since no independent rotational ground motion sensor with a comparable sensitivity is currently available in the vicinity of the TB, ground motion can only be assumed to be the origin of the measured dynamics. The signal, however, is coherent to  $CAP_{RZ}$  below 10 mHz, which indicates the detection of motion rather than sensor noise. As discussed above, no significant coherence to temperature fluctuations was observed above 0.4 mHz, see figure 6. Above about 100 mHz horizontal motion couples to the torsional measurement, which is limited at high frequencies by the sensor noise of the OL.

#### 4. Improving the HTB: discussion and outlook

The HTB is now in a state where it is well understood. Robust control and witness sensors are optimized for low-noise sensing and control of the suspended IM. Seismic noise is limiting our measurements over a wide frequency band. To mitigate the influence of seismic noise, the entire vacuum system is supported by three PZT feet. By feeding to these actuators the chamber motion signal, sensed with three seismometers, CAP and OL, the suspension point motion can be minimized. The three heavy duty PZTs currently installed are uni-axial and therefore allow for vertical and tilt control of the torsion fiber suspension point. Since the low frequency differential motion between IM and chamber is most probably dominated by tilt induced horizontal displacement, the three-point vertical control will be suitable to strongly reduce ground motion coupling. First tests using only the signals of the seismometers were conducted and promising suppression of vertical chamber motion was achieved. We are currently extending the system to include the optical signals as well. An upgrade to a 6 DoF actuation unit is planned for the future. The TMs, the IM structure, and the capacitor plates installed in the current configuration were made from uncoated aluminium for the sake of flexibility in terms of design changes and adaptations. For future iterations we foresee to incorporate gold-coated components in order to improve the conductivity and reduce effects of inhomogeneous electric fields and accumulated surface charges. Moreover, this will remove the need for the integration of gold-coated mirrors to obtain suitable reflectivities for probing the TMs with laser interferometers from multiple sides.

The next step towards the optical inertial sensor tests will be the integration of the first interferometric readout of the reinstalled third and fourth TM. This will not only improve the HTB sensitivity, but will also provide valuable information on the process for testing interferometric inertial sensors. Multi-DoF integrated optical sensing and electrostatic actuation units (see figure 1) will themselves allow for identifying and attenuating noise contributions. The analysis of angular seismic motion, for instance, will be better understood and counteracted by the PZT-feet.

Ultimately, suspension thermal noise will limit our TB. Increasing the Q-factor and thereby lowering the thermal noise amplitude by exchanging the tungsten suspension wire with, for instance, a fused silica fiber is currently being evaluated. Furthermore, an all-fused-silica monolithic fiber and IM structure is being discussed.

## 5. Conclusion

In this article, we introduce the HTB, a new TB facility for developing and testing novel, primarily optical, inertial sensors for future space missions. It is designed with the scope of being a versatile test bed for weak force measurements down to the mHz regime. Currently in the commissioning phase, the system has already yielded promising results based on initial sensitivity measurements. OLS and CAP sensors are employed to measure the dynamics of the IM. The OLS achieve a sensitivity of down to  $1.5 \cdot 10^{-10} \text{ rad } \sqrt{\text{Hz}}^{-1}$ , through a simple and robust optical setup. The CAP sensors, on the other hand, have slightly less sensitivity of down to  $9 \cdot 10^{-10} \text{ m } \sqrt{\text{Hz}}^{-1}$ , but provide a higher dynamic range and allow for simultaneous TM actuation. Their concept is closely related to conventional inertial sensor readout systems. Both optical levers and CAP sensors are therefore ideal to use as witness and control sensors in subsequent inertial sensor unit tests.

The HTB has been characterized by combining the information from the IM readout with that from a set of temperature sensors and seismometers. The temperature stability inside the vacuum system of down to  $11 \text{ mK } \sqrt{\text{Hz}}^{-1}$  at  $50 \mu\text{Hz}$  minimizes noise due to thermally induced structural deformations. As expected, ambient ground vibration induced motion of the vacuum chamber and the IM dominates the readout of the installed sensors over a wide frequency band. This fact has been exploited to study the potential of using our TB as a ground motion sensor. The development of low frequency multi DoF seismic motion sensors is crucial, for example, for improving ground based gravitational wave detectors. Due to the high susceptibility to low frequency ground vibrations, the HTB could contribute in this regard. By analyzing data from capacitive sensors and optical levers, upper limits have been derived for one horizontal DoF and the torsional DoF. Multi-DoF interferometric readout of the TMs will improve the ground motion sensing. Furthermore, an optimized geometry could allow for the design of 6 DoF ground motion sensors based on the experience with the HTB.

Currently, the HTB sensitivity is limited to  $5 \cdot 10^{-11} \text{ m s}^{-2} \sqrt{\text{Hz}}^{-1}$  at 4 mHz which is about a factor 500 above the estimated thermal noise limit of the system. The planned integration of interferometric readout will help to improve the current understanding of noise sources. Together with the suppression of seismic noise by the piezo actuators, we expect that substantial improvements in sensitivity are possible.

## Data availability statement

The data cannot be made publicly available upon publication because no suitable repository exists for hosting data in this field of study. The data that support the findings of this study are available upon reasonable request from the authors.

## Acknowledgments

The authors acknowledge funding and support by Deutsche Forschungsgemeinschaft (DFG, German Research Foundation) - Project-ID 434617780 - SFB 1464, Deutsche Forschungsgemeinschaft (DFG, German Research Foundation) - Project-ID 239994235 - SFB 1128, Deutsche Forschungsgemeinschaft (DFG, German Research Foundation) under Germany's Excellence Strategy—EXC-2123 QuantumFrontiers - 390837967, and the Max Planck Society (MPG) in the framework of the LEGACY cooperation on low-frequency gravitational wave astronomy (M.I.F.A.QOP18098).

## ORCID iDs

Gerald Bergmann  <https://orcid.org/0009-0005-7948-0290>  
 Carolin Cordes  <https://orcid.org/0009-0002-3534-8931>  
 Christoph Gentemann  <https://orcid.org/0009-0002-7207-3893>  
 Wang Qinglan  <https://orcid.org/0000-0002-6431-4477>  
 Gerhard Heinzl  <https://orcid.org/0000-0003-1661-7868>  
 Moritz Mehmet  <https://orcid.org/0000-0001-9432-7108>

## References

- [1] Landerer F W *et al* 2020 *Geophys. Res. Lett.* **47** e2020GL088306
- [2] Kornfeld R P, Arnold B W, Gross M A, Dahya N T, Klipstein W M, Gath P F and Bettadpur S 2019 *J. Spacecr. Rockets* **56** 931–51
- [3] Touboul P *et al* (MICROSCOPE Collaboration) 2022 *Phys. Rev. Lett.* **129** 121102
- [4] McNamara P, Vitale S and Danzmann K (behalf of the LISA Pathfinder Science Working Team) 2008 *Class. Quantum Grav.* **25** 114034
- [5] Armano M *et al* 2015 The lisa pathfinder mission *J. Phys.: Conf. Ser.* **610** 012005
- [6] Amaro-Seoane P *et al* 2017 Laser interferometer space antenna (arXiv:1702.00786)
- [7] Christophe B, Boulanger D, Foulon B, Huynh P A, Lebat V, Liorzou F and Perrot E 2015 *Acta Astronaut.* **117** 1–7
- [8] Touboul P, Foulon B, Lafargue L and Metris G 2002 *Acta Astronaut.* **50** 433–43
- [9] Dolesi R *et al* 2003 *Class. Quantum Grav.* **20** S99
- [10] Armano M *et al* 2018 *Phys. Rev. Lett.* **120** 061101
- [11] Armano M *et al* 2022 *Phys. Rev. D* **106** 082001
- [12] Heinzl G, Cervantes F G, Marín A F G, Kullmann J, Feng W and Danzmann K 2010 *Opt. Express* **18** 19076–86
- [13] Gerberding O 2015 *Opt. Express* **23** 14753–62
- [14] Isleif K S, Gerberding O, Mehmet M, Schwarze T S, Heinzl G and Danzmann K 2016 *J. Phys.: Conf. Ser.* **716** 012008
- [15] Isleif K S, Heinzl G, Mehmet M and Gerberding O 2019 *Phys. Rev. Appl.* **12** 034025
- [16] Schlamminger S, Choi K Y, Wagner T A, Gundlach J H and Adelberger E G 2008 *Phys. Rev. Lett.* **100** 041101
- [17] Luo J, Liu Q, Tu L C, Shao C G, Liu L X, Yang S Q, Li Q and Zhang Y T 2009 *Phys. Rev. Lett.* **102** 240801
- [18] Li Q *et al* 2018 *Nature* **560** 582–8
- [19] Gundlach J H and Merkowitz S M 2000 *Phys. Rev. Lett.* **85** 2869
- [20] Tan W H *et al* 2020 *Phys. Rev. Lett.* **124** 051301
- [21] Lee J, Adelberger E, Cook T, Fleischer S and Heckel B 2020 *Phys. Rev. Lett.* **124** 101101
- [22] Westphal T, Hepach H, Pfaff J and Aspelmeyer M 2021 *Nature* **591** 225–8
- [23] Campsie P, Hough J, Rowan S and Hammond G 2014 *Class. Quantum Grav.* **31** 175007
- [24] Cavalleri A *et al* 2009 *Class. Quantum Grav.* **26** 094017
- [25] Cavalleri A, Ciani G, Dolesi R, Hueller M, Nicolodi D, Tombolato D, Wass P, Weber W, Vitale S and Carbone L 2009 *Class. Quantum Grav.* **26** 094012
- [26] Russano G *et al* 2018 *Class. Quantum Grav.* **35** 035017
- [27] Ciani G, Chilton A, Apple S, Olatunde T, Aitken M, Mueller G and Conklin J W 2017 *Rev. Sci. Instrum.* **88** 064502
- [28] Dávila Alvarez A *et al* 2022 *J. Geod.* **96** 70
- [29] Apple S *et al* 2023 *Rev. Sci. Instrum.* **94** 054502
- [30] Nanometrics, Trillium Horizon 120 (available at: <https://nanometrics.ca/products/seismometers/trillium-horizon-120>)
- [31] Bartington, three-axis magnetic field sensor MAG-03MS250 (available at: <https://georeva.eu/wp-content/uploads/2021/02/Mag-03-DS0013-1.pdf>)
- [32] Bork R, Hanks J, Barker D, Betzwieser J, Rollins J, Thorne K and von Reis E 2021 *SoftwareX* **13** 100619

- [33] Saulson P R 2017 *Fundamentals of Interferometric Gravitational Wave Detectors* 2nd edn (World Scientific) (<https://doi.org/10.1142/10116>)
- [34] Chilton A, Shelley R, Olatunde T, Ciani G, Conklin J W and Mueller G 2015 The UF torsion pendulum, a LISA technology testbed: sensing system and initial results *J. Phys.: Conf. Ser.* **610** 012038
- [35] Buikema A *et al* 2020 *Phys. Rev. D* **102** 062003
- [36] Mow-Lowry C M and Martynov D 2019 *Class. Quantum Grav.* **36** 245006
- [37] Lück H (ET Editorial Team) 2020 *et al* Et design report update 2020 *Design Report Update 2020 for the Einstein Telescope* (available at: <https://apps.et-gw.eu/tds/?content=3&r=17245>)
- [38] Matichard F and Evans M 2015 *Bull. Seismol. Soc. Am.* **105** 497–510